Enhancing Lime-Based Mortars with Multiwalled Carbon Nanotubes – Composites for Historic Building Restoration: Mechanical, Thermal, and Hygric Performance Analysis

Adam Pivák , Martina Záleská , Milena Pavlíková , Zbyšek Pavlík *

Posted Date: 27 April 2025

doi: 10.20944/preprints202504.2222.v1

Keywords: hydrated lime; hydraulic lime; multiwalled carbon nanotubes; mechanical resistance; cultural heritage; drying rate

 doi:10.20944/preprints202504.2222.v1

Article

Enhancing Lime-Based Mortars with Multiwalled Carbon Nanotubes – Composites for Historic Building Restoration: Mechanical, Thermal, and Hygric Performance Analysis

Adam Pivák, Martina Záleská, Milena Pavlíková and Zbyšek Pavlík *

Department of Materials Engineering and Chemistry, Faculty of Civil Engineering, Czech Technical University in Prague, Thákurova 7, 166 29 Prague, Czech Republic; adam.pivak@fsv.cvut.cz (A.P.); martina.zaleska@fsv.cvut.cz (M.Z.); milena.pavlikova@fsv.cvut.cz (M.P.)

* Correspondence: pavlikz@fsv.cvut.cz; Tel.: +420-224-357-917

Abstract: The use of binders in construction dates back to antiquity, with lime-based materials historically playing a significant role. However, the 20th century brought the widespread replacement of lime with Portland cement (PC), for its superior mechanical strength, durability, and faster setting time. Despite these advantages, the restoration of historic masonry structures has revealed the incompatibility of PC with traditional materials, leading to damage due to increased brittleness, stiffness, and reduced permeability. Consequently, lime mortars remain the preferred choice for heritage conservation. To enhance their durability while maintaining compatibility with historic materials, the incorporation of carbon-based nanoparticles has gained attention. This study investigates the impact of the carbon nanotubes (CNTs) additive on two types of lime-based mortars, calcium lime (CL) and hydraulic lime (HL), evaluating structural and mechanical properties, heat transport characteristics, and hygric properties after modification by CNTs with the dosage of 0.1%, 0.3%, and 0.5% binder weight. Incorporation of CNTs into CL mortar resulted in an increase in mechanical strength and slight reduction in heat transport and water absorption due to changes in porosity. The addition of CNTs into HL mortars reduced porosity, pore size distribution, and other depending characteristics. The utilisation of CNTs as an additive in the investigated lime-based composites has been identified as a potentially effective approach for the reinforcement and functionalisation of these composite materials, as they exhibited enhanced mechanical resistance while preserving their other engineering properties, making them well-suited for use as compatible mortars in building heritage repairs.

Keywords: hydrated lime; hydraulic lime; multiwalled carbon nanotubes; mechanical resistance; cultural heritage; drying rate

1. Introduction

The application of binders in construction dates back to antiquity, when various materials based on clay, gypsum, or lime were utilised. Lime, obtained by burning limestone, which was abundant for masonry and plastering, is considered to be one of the oldest binders. However, from the early 19th and 20th century, hydraulic lime materials and Portland cement (PC) began to replace traditional lime binders [1-3]. Since then, PC has become the most widely used binder in the construction industry, with global production reaching billions of tons per year. In 2022, production exceeded 4 billion tons [4].

When comparing PC mortars with lime-based mortars, several significant differences can be observed. Portland cement-based composites exhibit higher mechanical strength, corrosion

 doi:10.20944/preprints202504.2222.v1

resistance, durability, and faster setting than lime-based materials. This makes them suitable for modern construction, where faster completion and high performance at an early age are required. This contributed to the decline of lime mortars. However, in some specific cases, the use of lime mortars is generally preferred. For instance, renders not only play aesthetic purposes but also a protective role in mitigating wall deterioration. Compared to PC, lime mortars are more permeable to water vapour. This makes traditional lime mortars more appropriate for the reconstruction of historic buildings, where their use, e.g., in the form of a "sacrificial" layer, ensures effective moisture regulation within the structure and consequently preventing potential damage to the original materials [5, 6].

In the 1990s, the restoration of masonry structures commonly involved replacing the original mortar with cement-based alternatives. Subsequent observations, however, revealed that these alterations and repairs were not well suited to historic masonry. This is attributed to the enhanced brittleness and stiffness of cement-based mortars, which is coupled with their reduced water vapour permeability [7]. These properties have been demonstrated to cause substantial damage to construction and built elements. Furthermore, the transfer of soluble salts from the cement mortar itself to the masonry substrate accelerated the deterioration process [8,9]. Therefore, it is essential that the restoration of historic buildings prioritizes compatibility with original materials to ensure that the structural integrity and authenticity of historic buildings will be preserved [10, 11].

In current practice, the selection of lime mortars as the primary restoration material is often attributed to their capacity to integrate with original inbuilt materials. This is particularly evident in scenarios that involve the restoration of original mortar application techniques, a process that inherently has historical and technical value. However, increasing demand for durable buildings has necessitated the modification of materials for repair of historic buildings to enhance their longevity while preserving their original functional properties and compatibility with existing structures. The incorporation of nanoscale materials has been identified as a promising approach to enhance the strength of materials and extending their lifespan.

The construction industry is increasingly focussing on the utilization of nanomaterials in building composites because of their potential to enhance various characteristics. A broad selection of nanomaterials is available, presenting a multitude of potential applications, including substantial enhancements in properties such as strength, durability, and sustainability. A significant class of nanomaterials that has attracted considerable attention is that of carbon-based nanomaterials, which has been widely studied, particularly in the properties of Portland cement concrete. Jeevanagoudar et al. [12] reported a 17% increase in compressive strength with the incorporation of 0.4 wt.% multiwalled carbon nanotubes (MWCNTs) into the material, although higher dosages led to a reduction in performance. In the research conducted by Dalla et al. [13], a 26% strength enhancement was observed with the incorporation of 1.0 wt% graphene nanoplatelets (GNs). Conversely, Chen et al. [14] achieved a 28% increase using only 0.04 wt.% GNs. In the case of lime-based composites, the research conducted by Dimou et al. [15, 16] on the properties of lime pastes-cement and natural hydraulic lime (NHL) revealed that the incorporation of modified MWCNTs resulted in a 10.6% enhancement in tensile strength, while the use of MgO-modified GO yielded a 20% increase in strength. Furthermore, Faria et al. [17] reported a 12.5% improvement in NHL mortar strength with 0.1 wt.% modified graphene.

The performance of composites is influenced not only by the properties of the nanomaterials (NMs) used, but also by their degree of dispersion within the composite, which can be complex due to the tendency of nanoparticles to form clusters held together by weak van der Waals forces, both in the dry state and in solutions [18]. If NMs are not uniformly dispersed, the formation of agglomerates creates weak points of interaction that reduce the final mechanical strength; therefore, overcoming aggregating forces is essential for proper distribution and incorporation of NMs into the material mixture. The effectiveness of the applied nanomaterials depends on factors such as the dispersion technique, chemical stabilisation, nanomaterial volume, and possible surface modifications. The most commonly used dispersion techniques include high-speed homogenisation and ultrasonication [19-

 doi:10.20944/preprints202504.2222.v1

21]. The ultrasonic method uses ultrasonic waves that break apart NM clusters by disrupting their surface layers, thereby overcoming van der Waals forces; the dispersion process can take minutes [22], hours [23], or even days [24]. In addition to the dispersion technique, the homogeneity and stability of the dispersion of NM can be enhanced by modifying the surface properties of the nanoparticles and using chemical agents, such as surfactants or solvents [25].

Given the limited research on enhancing the properties of lime-based composites, this study is focused on the evaluating the impact of incorporating carbon nanotubes (CNTs) into lime-based mortars. The objective is to determine the most effective method for dispersing and integrating the nanoadditive into fresh mixtures. A comprehensive series of tests was conducted to assess the structural properties, mechanical strength, heat transfer and storage characteristics, water absorption and ingress, as well as the drying capability of both the control and nano-enriched mortars. The research on nanomodified mortars aims to discover promising materials with improved properties to use as an alternative to mortars used commonly for repair of historic buildings. This approach aims to attain optimal performance by exploiting the unique properties of carbon nanotubes, which can significantly improve the structural integrity, mechanical strength, and durability of low-performance lime-based mortars. Considering that cultural heritage authorities generally do not oppose the use of carbon-based nanoparticles, the nano-enhanced lime-based composites can be used in scenarios where the use of Portland cement is restricted. The incorporation of CNTs represents thus a viable route to the development of high-performance lime-based mortars suitable for the restoration and preservation of historic buildings.

2. Materials and Methods

This experimental study investigates the potential for modifying lime mortars based on lime hydrate (CL) and hydraulic lime (HL) using carbon-based nanotubes. The paper includes a characterisation of both types of binder, filler, as well as design of mortar mixtures. In the case of the chosen nanoadditive, particular focus was given to the investigation of the effectiveness of several dispersion techniques and supporting chemical agents for their homogeneous distribution during the preparation of fresh mortar mixtures.

2.1. Materials and Sample Preparation

The studied mortars were composed of lime hydrate CL 90-S (Čertovy schody a.s., Lhoist group, Tmaň, Czech Republic) or hydraulic lime HL 5 (Baumit GmbH, Waldegg, Austria). As aggregate, silica sand (Filtrační písky s.r.o., Chlum u Doks, Czech Republic) composed of three fractions was used. The three fractions labelled as PG1 (0-0.5 mm), PG2 (0.5-1.0 mm) and PG3 (1.0-2.0 mm) were mixed in 1: 1: 1volume ratio to produce a filler with a total grain size of 0-2 mm. The quantity of filler was determined based on standard mortar strength tests, with a binder-to-filler ratio of 1:3 by weight. To ensure uniform workability across all mixtures, the quantity of batch water was adjusted so that the spread diameter of the fresh mixture, as assessed by the flow table test, conformed to the value of 165 ± 5 mm, which is a typical criterion for repair mortars intended for manual application.

As nanoadditive, industrial grade multi-walled carbon nanotubes TNIM8 (TimesNano, Chengdu, China) with a diameter of 30-80 nm and maximum length 10 μm were applied. Based on sources from the literature on nanomaterial modified composites and our previous studies on the modification of magnesia-based composites [26, 27], the incorporation of CNTs was chosen at doses of 0.1%, 0.3% and 0.5% by weight of the binder used (mixtures labelled CNT0.1, CNT0.3 and CNT0.5).

A similar mixing procedure was used to prepare both types of mortar. The first step was to disperse carbon nanotubes in part of batch water mixed with surfactant Triton X-100® (Carl Roth GmbH, Karlsruhe, Germany) and Antifoam A concentrate (Sigma-Aldrich, St. Luis, USA). in the case of nanomodified mixtures. The method used to select the nanoparticle dispersing technique and the chemical agents supporting the chemical agents is described in Section 3.2. The CNTs were dispersed for 10 minutes. After dispersion, nanosuspensions were mixed with binder and the remaining batch water using a planetary mixer (ELE International, Milton Keynes, UK) with subsequent addition of

 doi:10.20944/preprints202504.2222.v1

aggregate according to the EN 459-2 [28]. The complete composition of the prepared mortars is presented in Table 1.

Table 1. Composition design of studied mortars (in g).

Mortar Mix	Lime Hydrate	Hydraulic Lime	Water	Silica Sand	CNTs	Triton® X-100	Defoamer
CL-R	1500	-	1575	3 x 1500	-	-	-
CL-CNT0.1	1500	-	1620	3 x 1500	1.5	1.5	0.675
CL- CNT0.3	1500	-	1575	3 x 1500	4.5	4.5	2.025
CL- CNT0.5	1500	-	1545	3 x 1500	7.5	7.5	3.375
HL-R	-	1500	1015	3 x 1500	-	-	-
HL- CNT0.1	-	1500	1015	3 x 1500	1.5	1.5	0.675
HL- CNT0.3	-	1500	1015	3 x 1500	4.5	4.5	2.025
HL- CNT0.5	-	1500	1015	3 x 1500	7.5	7.5	3.375

The prepared mixes were placed in plastic prismatic moulds (40 mm × 40 mm × 160 mm) and demoulded after 48 h. The specimens were divided into two sets. One set of specimens was cured for 28 days in a climatic chamber at a temperature of T = (23 ± 2) °C and varied relative humidity (RH) conditions, depending on the type of binder used. CL mortars were cured at a RH = (60 ± 5) % to aid in carbonation and hardening, while the relative humidity of the curing of the HL mortars was much higher (90 ± 5) % to allow the samples to hydrate and prevent the development of drying cracks. The second set of specimens was allowed to cure in similar conditions for 28 days and then left under laboratory conditions at T = (23 ± 2) °C and RH = (40 ± 5) % for a total of 90 days.

2.2. Evaluation of the Nanoadditive Dispersion Technique

In addition to the properties of the nanomaterials themselves, the uniform distribution of the particles in the mixture also influences the resulting properties of the nano-modified composites. Insufficient dispersion of the nanoadditive in the composite matrix leads to the formation of clusters held together by weak attractive van der Waals forces, resulting in the formation of weak spots, degrading the final material properties, and insufficient utilisation of the excellent properties of NMs. For this reason, the development of an efficient process for the preparation of carbon nanotube dispersions is required. Among the technological methods for the dispersion of NMs selected on the basis of studies [19-22], the method of mixing with high shear force stirrer UltraTurrax T-18 (IKA-Werke GmbH & Co. KG, Staufen, Germany) and sonication with ultrasonic bath Elmasonic Easy 60 H (Elma Schmidbauer GmbH, Singen, Germany) were used and tested. Based on other studies [29-31] investigating the use of chemical agents, it was decided that homogenisation will be enhanced by adding a stabilising non-ionic surfactants polysorbate 80 (commercial name Tween® 80) and octylphenol ethoxylate (Triton® X-100) and due to the formation and stabilisation of a foam Silicone Antifoam solution (Antifoam A) from Sigma-Aldrich (St. Louis, MO, USA). The amount of defoamer was measured using the foamability test [32], that is, measuring the volume of stabilised foam. The final amount was determined to ensure that the nanosuspension did not foam, which would have increased the total porosity of the mixture and final hardened material [33].

The degree of dispersion of the nanoadditives achieved by each technique was evaluated on the basis of visible light absorption, which was measured using a UV/VIS instrument GENESYS 30 Visible Spectrophotometer (Thermo Scientific™, Waltham, MA, USA). The evaluation assumed that when nanoparticles disperse in a liquid, their surface absorbs UV and visible light passing through the liquid. As the nanoparticles became more dispersed in the suspension, more of their surface area was exposed, and a higher level of absorption was measured at each wavelength.

 doi:10.20944/preprints202504.2222.v1

2.3. Characterization of Binders and Aggregate

The gravimetric method was used to determine the loose bulk density of all raw materials. The specific gravity was determined by helium pycnometry using a Pycnomatic ATC apparatus (Thermo ScientificTM, Waltham, MA, USA). The specific surface area was measured using an air permeability test using a Blaine UTCM-0280 automatic device (UTEST, Ankara, Turkey). The chemical composition of the binders used and that of the silica sand was determined using an ARL Quant'X EDXRF spectrophotometer (Thermo Scientific™).

Two methods were used to analyse the particle size distribution. The choice of method depended on the maximum particle size of the material studied. The particle size of finer binders was analysed by a laser diffraction technique using Analyssete 22 Micro Tec plus (FRITSCH GmbH, Weimar, Germany). For silica sand, the EN 1015-1 [34] sieving method was used as the particle size was larger.

2.4. Methods of Testing Fresh and Hardened Mortars

The workability of the fresh mortars was characterised by a flow table test according to EN 1015-3 [35]. The mortars cured for 28 days were used to determine basic physical properties and mechanical parameters. In addition, the characteristics of 90-days cured mortars were studied. Except mechanical and macrostructural parameters, the tests included MIP analysis, the evaluation of heat transfer and storage parameters, assessment of hygric characteristics and drying rate monitoring.

The basic structural characteristics of mortars that hardened in both curing regimes, 28-day and 90-day samples, were tested on 5 specimens dried in a vacuum chamber at 60 °C, until a steady state mass was reached. The measured parameters were bulk density, specific density, and open porosity. The measurement of the bulk density was carried out in accordance with the EN 1015-10 [36] standard using the gravimetric method. Specific density was determined using the pycnometric method (see Section 2.3). From the resulting bulk density and the specific density values obtained in the previous tests, the total open porosity was calculated. In addition to the previous tests, the samples cured for 90-days were subjected to a detailed characterisation of the porous structure by mercury intrusion porosimetry (MIP) using Pascal MIP 140 and 440 (Thermo Scientific™) measurement modules.

Testing of the parameters describing the mechanical strength of the tested mortars, namely flexural strength and compressive strength, was carried out according to EN 1015-11 [37] using a FP 100 mechanical press (Heckert, Rauenstein, Germany). To determine the flexural strength, the specimen (40 mm × 40 mm × 160 mm) was subjected to a three-point bending test with a support distance of 100 mm. Fragments from this test were used to determine compressive strength. The loading area in the uniaxial compressive strength test was 40 mm × 40 mm. Young's modulus was calculated based on the detection of the ultrasonic wave velocity as specified in EN 12504-4 [38]. The test was carried out by an ultrasonic testing apparatus Vikasonic (Schleibinger Geräte GmbH, Buchbach, Germany). Prior the testing, the specimens were dried in a vacuum chamber as the moisture presence would affect the measurement accuracy.

The thermal parameters tested were the dry thermal conductivity and the volumetric heat capacity. Data were acquired using a TPS 1500 HotDisk instrument (HotDisk AB, Gothenburg, Sweden). Using the capillary water absorption test [39, 40], the water absorption coefficient, the water absorption after 24-hour immersion and the apparent water diffusivity were determined.

Table 2 shows a summary of the experimental tests that were performed on cured mortars. In addition, it provides a comprehensive overview of the test methods that were exploited, along with the expanded combined uncertainties of the assessment of examined material parameters.

Table 2. A summary of the experimental tests carried out on hardened mortars.

Property	Symbol	Unit	ECU (%)	Standard /method
Bulk density	ρ_b	kg·m^{-3}	1.4	EN 1015-10 [36]

 doi:10.20944/preprints202504.2222.v1

Specific density	ρ_m	kg·m^{-3}	1.2	He pycnometry
Open porosity	ψ	%	2.0	EN 1015-10/He pycnometry
Pore size diameter	d_p	cm^3·g^{-1}	-	Mercury intrusion Porosimetry (MIP)
Average pore diameter	d_a	µm	-	MIP
Pore size distribution	*PSD*	%	-	MIP
Flexural strength	f_f	MPa	1.4	EN 1015-11 [37]
Compressive strength	f_c	MPa	1.4	EN 1015-11 [37]
Young´s modulus	E	GPa	2.3	EN 12504-4 [38]
Thermal conductivity	λ	W·m^{-1}·K^{-1}	2.3	Transient pulse technique
Volumetric heat capacity	C_V	MJ·m^{-3}·K^{-1}	2.3	Transient pulse technique
Water absorption coefficient	A_w	kg·m^{-2}·s$^{-1/2}$	2.3	EN 1015-18 [39]
24-hour water absorption	W_{a24}	kg·m^{-2}	1.4	EN 1015-18 [39]
Apparent moisture diffusivity	κ	m^2·s^{-1}	2.3	EN 1015-18 [39]
Phase 1 drying rate	D_1	kg·m^{-2}·h^{-1}	-	EN 16322 [41]
Phase 2 drying rate	D_2	kg·m^{-2}·h$^{-1/2}$	-	EN 16322 [41]
Drying index	*DI*	-	-	EN 16322 [41]

*ECU – expanded combined uncertainty.

The drying rate and drying index were measured on cubic samples (40 mm) cured for 90 days. First, the specimens were completely immersed in water until they were completely saturated, then covered on all sides with a vapour permeable film, except for one which was subjected to a controlled environment of T = (23 ± 2) °C and RH = (50 ± 5) % and served as an evaporation surface. The drying rate was calculated according to the standard EN 16322 [41] from the periodically recorded mass of the sample.

3. Results

3.1. Characterisation of Raw Materials

As shown in Table 3, the main chemical component of both binders is CaO. High concentrations of CaO are typical, especially for lime hydrate. Additionally, a higher content of hydraulic oxides (SiO_2, Al_2O_3, Fe_2O_3) was also observed in the hydraulic lime. In the case of the aggregate used, quartz was identified as the main component of the silica sand. Furthermore, the presence of Al_2O_3 was also detected.

Table 3. Results of the XRF analysis of the binders and aggregate.

Material	Lime Hydrate	Hydraulic Lime	Silica sand
CaO	95.31	57.84	0.01
Al_2O_3	3.07	11.63	3.23
SiO_2	0.27	20.45	96.34
MgO	1.22	1.47	0.35
Fe_2O_3	0.06	1.78	0.04
SrO	0.04	0.05	-
NiO	0.03	-	-
Na_2O	-	2.38	-
K_2O	-	2.32	0.01

 doi:10.20944/preprints202504.2222.v1

SO_3	-	1.43	0.01
MnO	-	0.32	-
TiO_2	-	0.26	0.01
ZrO	-	0.07	-
∑	100.00	100.00	100.00

Table 4 shows the basic physical characteristics of the raw materials used. The lime hydrate had a significantly higher fineness and lower loose bulk density compared to hydraulic lime. The Blaine specific surface area of the silica sand was not measured due to its coarser character.

Table 4. Basic physical characteristics of used binders and aggregate.

Material	Loose Bulk Density ($kg \cdot m^{-3}$)	Specific Density ($kg \cdot m^{-3}$)	Blaine Specific Surface ($m^2 \cdot kg$)
Lime hydrate	445	2228	1655
Hydraulic lime	788	2625	358
Silica sand	1671	2646	-

The particle size distribution parameters d_{90}, d_{50}, and d_{10} for lime hydrate were recorded as 88.3 μm, 46.3 μm, and 3.7 μm, respectively. Conversely, the parameters for hydraulic lime were measured at 63.4 μm, 34.7 μm, and 19.3 μm. The increased porosity attributed to the loose bulk density of lime hydrate particles, in contrast to those of hydraulic lime, is identified as the underlying factor for its markedly higher Blaine fineness. This high porosity also rendered the comparison of particle size distribution parameters ineffective for determining which binder exhibited greater fineness. The granulometry curve of the silica aggregate is shown in Figure 2.

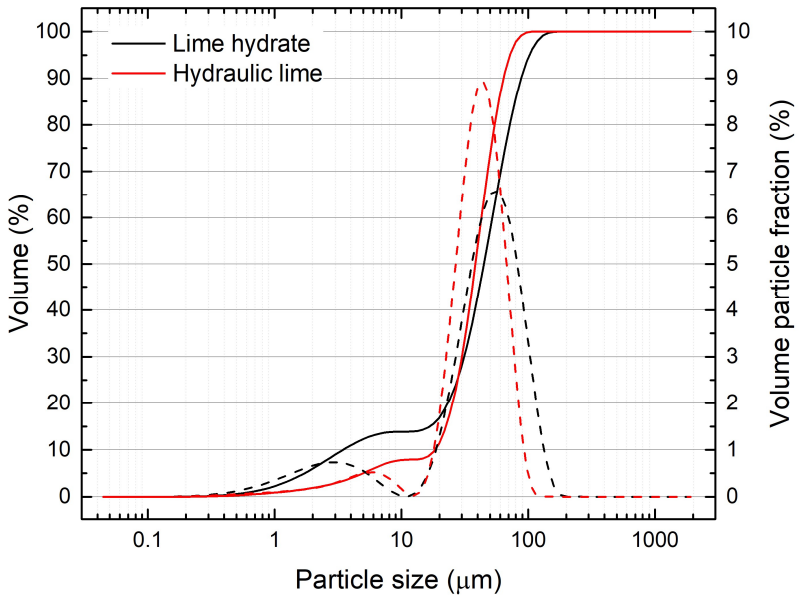

Figure 1. Particle size distribution of used binders.

 doi:10.20944/preprints202504.2222.v1

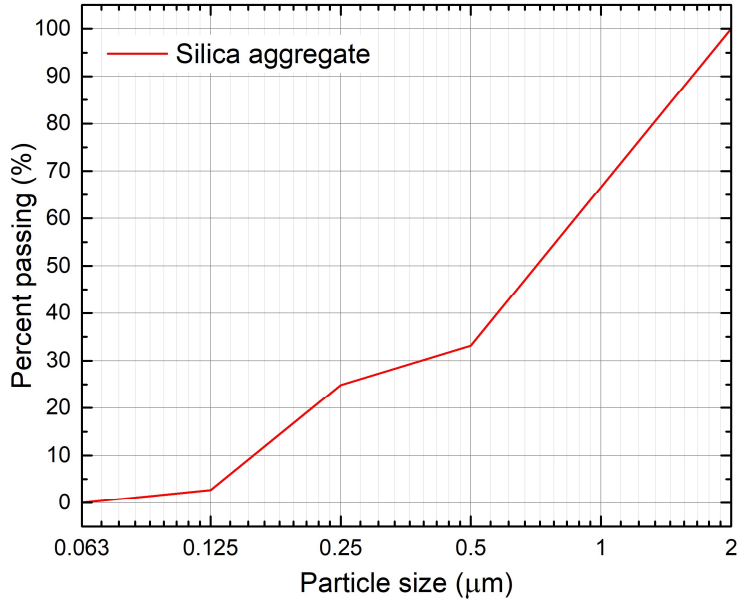

Figure 2. Granulometry curve of silica aggregate.

3.2. Dispersion Techniques

The results of the foamability test, evaluated as the quantity of defoamer (surfactant/defoamer ratio) in relation to the volume of stabilised foam, can be seen in Figure 3, which shows the higher efficiency of the chemical agent Triton® X-100 in forming and stabilising foam compared to Tween® 80. A significant reduction in foam amount was achieved with just 5 wt.% of defoamer. No foam stabilisation was observed with Tween® 80 and 30 wt.% defoamer. In the case of Triton® X-100, it was necessary to use a higher amount of defoamer, 40% by weight of surfactant, to stop the forming of foam completely.

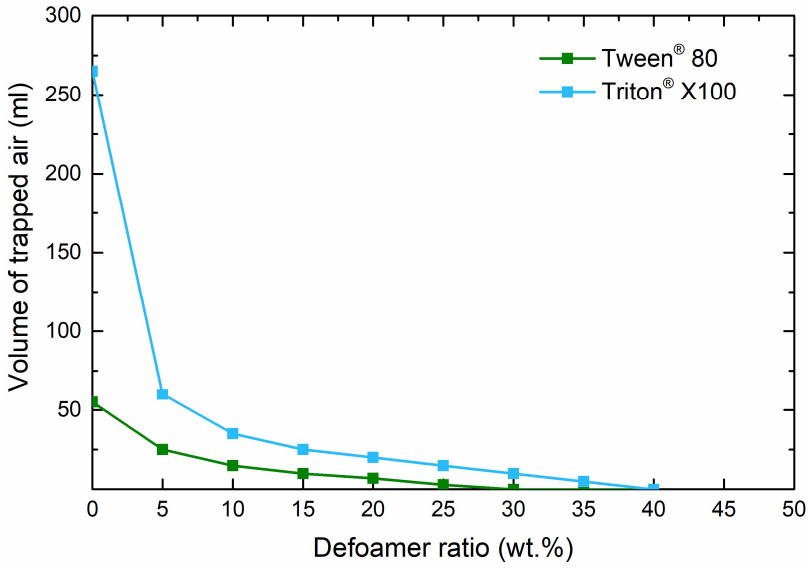

Figure 3. Foam stabilisation of surfactant solutions with defoamer.

Figure 4 presents the effectiveness of the dispersion techniques that were tested for the dispersion of CNTs in tap water and surfactant solutions. The results show that the nanosuspension dispersion carried out by sonication supported with Triton® X-100 and defoamer achieved the highest UV light absorbance at all wavelengths, which indicates that this method is the most effective. The

 doi:10.20944/preprints202504.2222.v1

other methods used were much less effective, in particular homogenizing using a high-shear mixer, which was the worst no matter what chemicals were used.

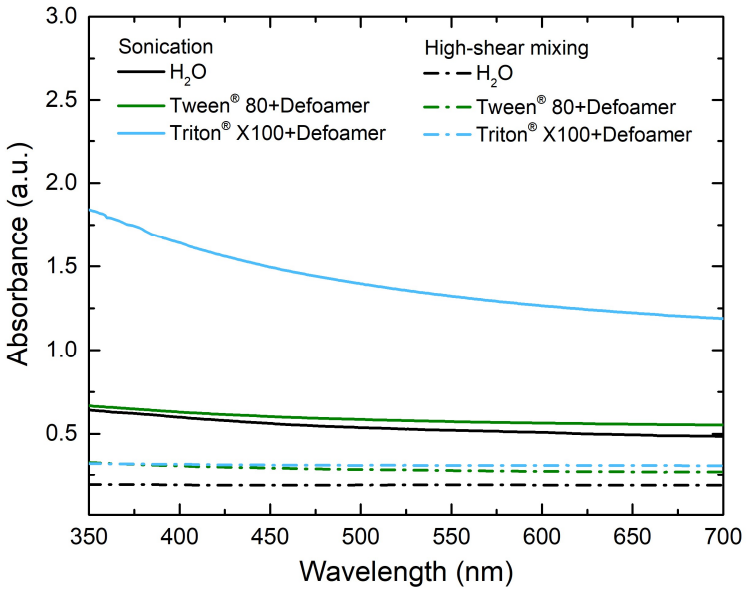

Figure 4. UV/VIS absorption spectra of CNTs solutions.

3.2. Properties of 28-day and 90-day Hardened Mortars

Table 5 presents the basic structural properties of the mortars cured for 28 and 90 days. The addition of CNTs in CL mortars resulted in a decrease of the 28-day bulk density and an increase in porosity by approx. 2% (absolute value). In the case of specific density and differences between individual modified CL mortars, the nanoadditive had only a minor effect on investigated basic structural parameters. The differences were in most cases within the range of the uncertainty of the measurement. As a result of the prolonged carbonation of 90 days cured lime mortars, the samples showed a slight increase in bulk density and matrix density values followed by a distinct decrease in porosity, as compared to 28-day samples. In case of CL mortars with CNTs, the reduction in porosity due to the prolonged curing time was significantly higher than observed for reference material CL-R and was ranging from 1.4% to 2.0% (absolute porosity values).

When CNTs were added to HL mortar, the bulk density increased by more than 9 % when 0.1% and 0.3% nanoadditive dosage were added and by 8% with 0.5% dosage applied. The resulting open porosity values of HL mortars were reduced by approximately 6 % (in absolute terms) compared to the pure hydraulic lime sample. Only minor, quantitatively unessential differences between structural parameters of 28-day and 90-day samples of HL mortars were recorded.

Table 5. Basic structural characteristics of hardened mortars.

Mortar	Bulk Density ρ_b (kg·m^{-3})		Specific Density ρ_s (kg·m^{-3})		Porosity ψ (%)	
	28 Days	90 Days	28 days	90 Days	28 Days	90 Days
CL-R	1656 ± 23	1675 ± 23	2545 ± 31	2552± 31	34.9 ± 0.7	34.4 ± 0.7
CL-CNT0.1	1599 ± 22	1618 ± 23	2535 ± 30	2548 ± 31	36.9 ± 0.7	35.0 ± 0.7
CL-CNT0.3	1617 ± 23	1659 ± 23	2537 ± 30	2550 ± 31	36.3 ± 0.7	34.9 ± 0.7
CL-CNT0.5	1601 ± 22	1659 ± 23	2538 ± 30	2549 ± 31	36.9 ± 0.7	34.9 ± 0.7
HL-R	1740 ± 24	1754 ± 25	2575 ± 31	2577 ± 31	32.4 ± 0.6	31.9 ± 0.6
HL-CNT0.1	1900 ± 27	1908 ± 27	2578 ± 31	2599 ± 31	26.3 ± 0.5	26.6 ± 0.5
HL-CNT0.3	1893 ± 27	1902 ± 27	2563 ± 31	2596 ± 31	26.2 ± 0.5	26.7 ± 0.5
HL-CNT0.5	1881 ± 26	1902 ± 27	2547 ± 31	2597 ± 31	26.2 ± 0.5	26.8 ± 0.5

 doi:10.20944/preprints202504.2222.v1

The effect of the addition of CNTs on the pore volume and pore size analysed with MIP is shown in Table 6. In the case of CL mortars, the control sample had an average pore diameter of approximately 0.2 μm, and a total pore volume that exceeded 0.16 $cm^3 \cdot g^{-1}$. An increase in both parameters was observed for all CL mortars modified with the CNT additive, which well corresponds with macrostructural data shown above. As illustrated in Figure 5, the dashed lines represent the cumulative pore size distribution curves, while the solid lines represent the incremental pore size distribution curves. The figure shows that the highest pore volumes of CL mortars were recorded in the range between 0.03 μm to 1 μm (capillary pores) and in the pore size corresponding to mascropores (> 10 μm).

Table 6. Microstructural characteristics of 90-day mortars obtained by MIP.

Mortar	Total Pore Volume d_p ($cm^3 \cdot g^{-1}$)	Average Pore Diameter d_a (μm)
CL-R	0.165	0.197
CL-CNT0.1	0.181	0.218
CL-CNT0.3	0.174	0.212
CL-CNT0.5	0.180	0.219
HL-R	0.183	0.068
HL-CNT0.1	0.110	0.055
HL-CNT0.3	0.113	0.058
HL-CNT0.5	0.117	0.063

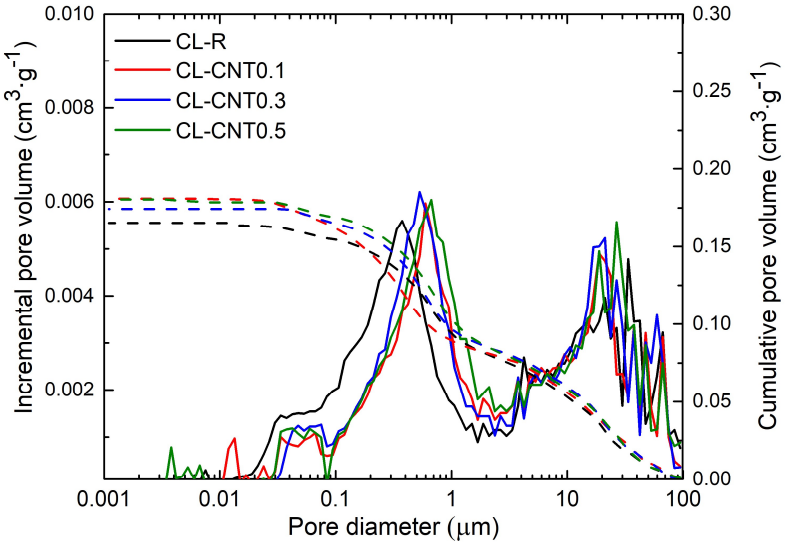

Figure 5. Pore size distribution of CL mortars, 90-day samples.

According to the pore size distribution demonstrated in Figure 6, an analysis of HL mortars indicated the prevalence of comparatively smaller pores compared to those observed in CL mortars. The majority of the pores were within the range of 0.02 μm to 0.25 μm. The average pore diameter of HL-R mortar was 0.068 μm and it was further reduced by the addition of CNTs into mortar mixes. It must also be considered that compared to the control mortar HL-R, hydraulic lime mortars containing CNTs had a significantly lower total pore volume, thus open porosity, and most of capillary pores with diameter around 0.06 μm, which can further decrease the rate of water ingress.

 doi:10.20944/preprints202504.2222.v1

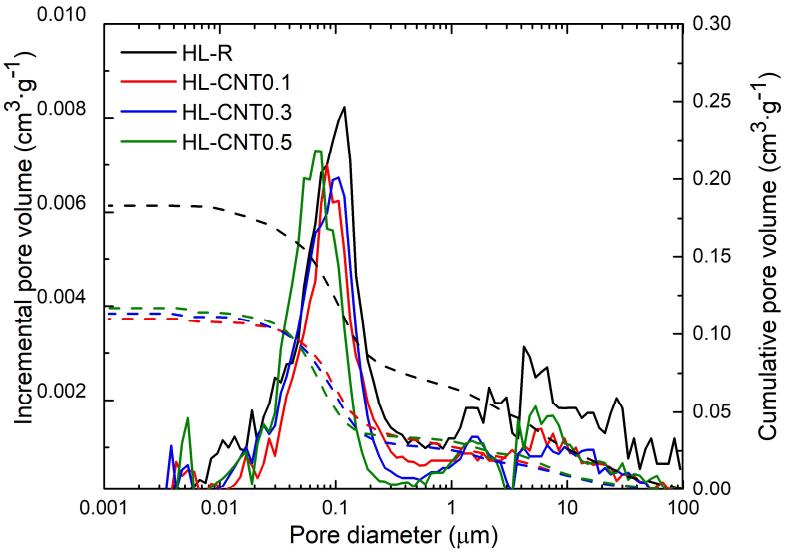

Figure 6. Pore size distribution of HL mortars, 90-day samples.

Table 7 shows the mechanical resistance of the hardened CL and HL mortars, characterised by flexural strength, compressive strength, and dynamic modulus of elasticity. The measurement results show that the flexural and compressive strengths of 28 days cured CL-R and CL-CNT0.1 mortars are identical, indicating that the 0.1% CNT addition does not significantly affect these mechanical properties. Nevertheless, even for the lowest dosage of CNTs, the increase in mechanical strength was observed after prolonged curing. The highest values of both flexural and compressive strength were observed for the CL-CNT0.3 mortar. The compressive strength exhibited an approximate increase of 30.9% for the 28-day sample and approximately 22.5% for the 90-day sample. Conversely, the enhancement in flexural strength was minimal, showing an improvement of merely 2% in comparison to the control sample cured for 90 days. It should be noted that for mortar CL-CNT0.5, both the flexural strength and the compressive strength were lower than those recorded for the control mortar, indicating a possible negative effect of the higher content of CNTs on mechanical performance due uneven dispersion of nanoadditive.

Modification of HL mortars with CNTs resulted in an overall, and quantitatively high improvement in mechanical parameters. Among the tested samples, HL-CNT0.3 exhibited the highest flexural and compressive strength. Specifically, the flexural strength was increased by nearly 19%, while the compressive strength showed a significant improvement of about 65.3% compared to the control sample. However, further increase in CNT dosage caused both parameters to decrease, suggesting that excessive CNT content may have a detrimental effect, as in the case of CL mortars.

The elasticity modulus of Cl mortars enriched by CNTS decreased by approx. 12 %. However, the addition of CNTs to HL mortars had more prominent effect. The elasticity modulus increased by maximum of 16.5 % when 0.1 CNT was applied after 28 days and by nearly 18 % after 90 days of curing. The observed results can be attributed to the excellent properties of the CNTs, as well as the solidified structure of the HL mortar. Similarly to the results of the compressive strength test, these properties contribute significantly to the improvement of the dynamic modulus of elasticity.

Table 7. Mechanical characteristics of hardened mortars.

Mortar	Flexural Strength f_f (MPa)		Compressive Strength f_c (MPa)		Dynamic Modulus of Elasticity E (GPa)	
	28 Days	90 Days	28 Days	90 Days	28 Days	90 Days
CL-R	0.48 ± 0.01	0.86 ± 0.01	0.55 ± 0.01	1.86 ± 0.03	4.2 ± 0.1	4.5 ± 0.1

 doi:10.20944/preprints202504.2222.v1

CL-CNT0.1	0.48 ± 0.01	0.82 ± 0.01	0.55 ± 0.01	1.98 ± 0.03	3.3 ± 0.1	3.7 ± 0.1
CL-CNT0.3	0.51 ± 0.01	0.88 ± 0.01	0.72 ± 0.01	2.28 ± 0.03	3.5 ± 0.1	3.7 ± 0.1
CL-CNT0.5	0.39 ± 0.01	0.77 ± 0.01	0.44 ± 0.01	1.95 ± 0.03	3.2 ± 0.1	3.4 ± 0.1
HL-R	2.16 ± 0.03	2.33 ± 0.03	7.43 ± 0.10	10.20 ± 0.14	10.3 ± 0.3	10.7 ± 0.3
HL-CNT0.1	2.42 ± 0.03	2.45 ± 0.04	11.78 ± 0.16	14.36 ± 0.20	12.0 ± 0.3	12.2 ± 0.3
HL-CNT0.3	2.57 ± 0.04	2.60 ± 0.03	12.28 ± 0.17	16.79 ± 0.24	11.9 ± 0.3	12.1 ± 0.3
HL-CNT0.5	2.42 ± 0.03	2.24 ± 0.03	11.27 ± 0.16	14.65 ± 0.21	11.5 ± 0.3	11.7 ± 0.3

The addition of CNTs also affected the heat transfer and storage properties. As shown in Table 8, for CL mortars, the thermal conductivity and heat capacity changed slightly depending on the CNTs dose as the CL-CNT and control samples had at 90-days almost identical total porosity. Although both thermal conductivity and heat capacity decreased with 0.1% nanoadditive, due to the great thermal conductivity of CNTs (2800-6000 $W \cdot m^{-1} \cdot K^{-1}$) [42] both parameters increased with higher CNTs content in the mix. The highest thermal conductivity and heat capacity of the modified CL mortars was recorded for 0.5 % CNT additive. In comparison to the control sample, both parameters exhibited a slight decrease; however, this reduction was confined within the bounds of measurement uncertainty.

For HL samples, both the thermal conductivity and the volumetric heat capacity values increased with the increasing volume of the nanoadditive applied. The most noticeable increase in both tested parameters was observed for CL-CNT0.5. (approx. 15% and 22% respectively). The variations in thermal parameters among the HL samples with varying concentrations of CNTs were relatively minor. However, generally, an increased dosage of CNTs resulted in increased heat transport and storage. This primary effect is attributable to a combination of reduced total porosity of the HL mortars and the intrinsic thermal properties of the CNTs used.

Table 8. Thermal characteristics of hardened mortars.

Mortar	**Thermal Conductivity λ ($W \cdot m^{-1} \cdot K^{-1}$)**	**Volumetric Heat Capacity C_v x 10^6 ($J \cdot m^{-3} \cdot K^{-1}$)**
CL-R	1.125 ± 0.026	1.176 ± 0.027
CL-CNT0.1	1.056 ± 0.024	1.153 ± 0.027
CL-CNT0.3	1.094 ± 0.025	1.174 ± 0.027
CL-CNT0.5	1.096 ± 0.025	1.182 ± 0.027
HL-R	1.107 ± 0.025	1.070 ± 0.025
HL-CNT0.1	1.248 ± 0.029	1.312 ± 0.030
HL-CNT0.3	1.252 ± 0.029	1.323 ± 0.030
HL-CNT0.5	1.280 ± 0.029	1.362 ± 0.031

Table 9 and Figure 7 present the results of the water absorption rate, the 24-hour water intake and the water absorption curves of the samples that were cured for 90 days. The water absorption coefficient of the control CL mortar was about 0.3, which is typical for this type of mortar. In contrast, HL mortars exhibited an absorption rate that was about 3.5 times less than that of CL mortars. This substantial decrease in water uptake was attributable to the reduced volume of accessible capillary pores for water transport as observed in MIP analysis and to the inherent nature of HL mortar, which is a blend of hydraulic lime and Portland cement, resulting in an inferred lower capacity for water movement.

A comparison of control samples of CL and HL mortars with the respective mixtures modified with CNT revealed only minor changes in all parameters. In every instance, the difference was in the range of the total combined uncertainty of the tests. This suggests that the inherent water transport behaviour of both types of mortars was preserved. With respect to water transport parameters, CL-based materials have demonstrated their suitability for the restoration of historic buildings [43].

 doi:10.20944/preprints202504.2222.v1

Table 9. Water absorption characteristics of the mortars cured for 90 days.

Mortar	Water Absorption Coefficient A_w ($kg \cdot m^{-2} \cdot s^{-1/2}$)	24 h Water Absorption W_{a24} ($kg \cdot m^{-2}$)
CL-R	0.31 ± 0.01	9.40 ± 0.13
CL-CNT0.1	0.30 ± 0.01	9.47 ± 0.13
CL-CNT0.3	0.30 ± 0.01	9.44 ± 0.13
CL-CNT0.5	0.30 ± 0.01	9.65 ± 0.14
HL-R	0.08 ± 0.01	8.73 ± 0.12
HL-CNT0.1	0.08 ± 0.01	8.78 ± 0.12
HL-CNT0.3	0.07 ± 0.01	8.75 ± 0.12
HL-CNT0.5	0.07 ± 0.01	8.59 ± 0.12

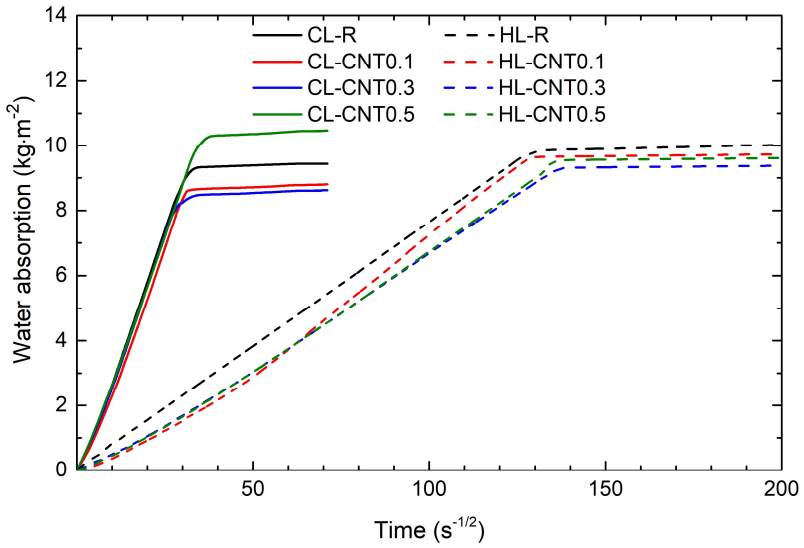

Figure 7. Capillary water absorption curves of hardened mortars, 90-day samples.

The one-dimensional drying process of 90-day mortars was represented by two phase-dependent drying rates, designated D_1 and D_2, and by the drying index (DI), evaluated from the total duration of the drying process and the total volume of evaporated moisture. The first phase of drying began immediately at the start of the measurement when the sample was fully saturated, and moisture was evaporating from the saturated surface exposed to the control environment. This phase is also referred to as constant drying rate [44], as illustrated in Figure 8A as a linear trend of moisture desorption as a function of time (h). The first drying rate (D1) is calculated as the gradient of the linear segment (to approx. 5 hours). The second phase is characterised by the nonlinear portion of the drying curve. The progress of surface evaporation leads to the transition of the evaporation front into the sample. Then evaporation consists of two components: water evaporation and moisture transport to the material surface. To quantify this phase, the drying process of the material was plotted against the square root of time ($h^{1/2}$) in Figure 8B, and the drying rate (D2) was obtained as the slope of its linear segment.

 doi:10.20944/preprints202504.2222.v1

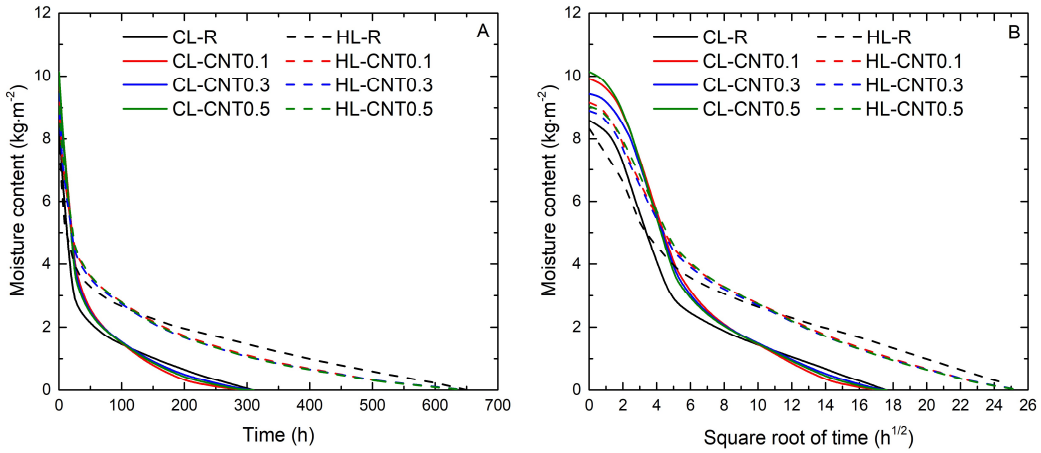

Figure 8. Evaporation curves of hardened mortars as a function of time (A); square root of time (B).

Table 10. The water desorption characteristics of mortars cured for 90 days.

Mortar	Phase 1 Drying Rate D_1 ($kg \cdot m^{-2} \cdot h^{-1}$)	Phase 2 Drying Rate D_2 ($kg \cdot m^{-2} \cdot h^{-1/2}$)	Drying Index *DI* (-)
CL-R	0.36	1.57	0.15
CL-CNT0.1	0.29	1.64	0.15
CL-CNT0.3	0.29	1.60	0.15
CL-CNT0.5	0.31	1.75	0.14
HL-R	0.26	0.88	0.19
HL-CNT0.1	0.32	1.05	0.16
HL-CNT0.3	0.30	1.11	0.16
HL-CNT0.5	0.27	1.13	0.16

Although the results of the capillary water absorption study were for CL mortars almost identical, the differences in the drying parameters were more noticeable. It was observed that in the case of CL mortars modified with CNTs, the first-phase drying rate decreased slightly. Conversely, an enhancement was noted in the drying rate during the second phase, suggesting an increased water vapour permeability in the nanotube-modified CL-CNT mortars during a subsequent stage of the drying process. It is hypothesized that this may be attributed to the slight alteration of the mortars' porous structure due to the presence of disruptive moisture. However, the overall drying performance characterized by DI, the value representing both volume of total moisture evaporation and evaporation time, was identical for CL control samples and CNTs modified mortars, regardless of the nanoadditive dosage.

Several significant differences were observed between the control mortars and the modified HL mortars. The incorporation of CNT into the porous structure of the mortars has been shown to accelerate the evaporation process and enhance the transport of water vapour during both phases of the drying process. The findings of this study are consistent with those of previous research [45, 46], particularly with respect to the observed water absorption characteristics. It is notable that the overall drying performance presented by DI shows an enhancement compared to the HL-R sample, while the variations between samples containing different doses of CNT were minimal, indicating that the drying performance was primarily influenced by the presence of nanomaterials rather than their specific dosage. In is necessary to emphasise, the higher the drying index, the more difficult it becomes for the material to lose water to the environment [47].

 doi:10.20944/preprints202504.2222.v1

4. Conclusions

The presented study focused on the modification of lime-based mortars through the incorporation of multi-walled carbon nanotubes. The methodology for the integration of CNTs in the composite mixture was developed, and the effect of this nanoadditive on the structural, mechanical, thermal, hygric, and drying properties of the hardened mortars was tested. A summary of the key results from the conducted experiments is given below.

(1) The UV/VIS spectroscopy test and the foamability test demonstrated that the most effective technique for producing nanosuspensions is the dispersion of nanotubes in an ultrasonic bath with the addition of surfactant and defoamer.

(2) The incorporation of CNTs resulted in the decreased bulk density and 2% increase in porosity of CL mortars, with no significant impact on the specific density. In contrast, the density of HL mortars exhibited an increase more than 9% (0.1% and 0.3% dosage) and 8% (0.5% dosage), while open porosity showed decrease of 6% compared to the reference hydraulic lime samples. Following a prolonged curing period, a slight increase in bulk and matrix density was observed with a small decrease in porosity.

(3) The water absorption and drying behaviour of CL mortars exhibited no significant changes between the control and modified mortars. The capillary water absorption of the HL mortars was minimal, but significant differences were observed in the drying process. Nano-modification of the HL mortars resulted in accelerated drying (evaporation) and enhanced water vapour transfer.

(4) In the case of CL mortars, the thermal conductivity and volumetric heat capacity showed minor variations due to similar porosity. In HL mortars, both parameters consistently increased with the content CNTs, with maximum increases of 15 %, and 22 % respectively, at 0.5% CNTs dosage. This effect was linked to the reduced porosity in HL mortars and the high thermal conductivity of CNTs themselves.

(5) The beneficial properties of CNTs incorporated into mortars were evident in the mechanical strength assessment. While the 0.1% dose of CNTs exhibited minimal impact on CL mortar, the application of a higher dose (0.3%) led to a substantial enhancement in the compressive strength, surpassing 30% for 28-days cured samples. The modified HL mortar exhibited an enhancement across all applied volumes. A significant effectiveness was observed when 0.3% of CNTs was incorporated, resulting in an increase of the compressive strength exceeding 65 % and nearly 19% improvement of the flexural strength. The extended duration of the curing process led to an improvement in the strength parameters of all samples, resulting in the maximum compressive strengths of 2.28 MPa (CL) and 16.79 MPa (HL) when a volume of 0.3% CNTs was used.

Incorporation of carbon nanotubes as a nanoadditive has shown great promise in improving the durability of mortars. The exceptional properties of CNTs contribute to the improved mechanical strength while maintaining the original properties of the mortars, ensuring their compatibility with traditional structures and inbuilt materials. In this regard, improvement of mechanical strength of CL mortar, which is usually low, represent unexceptionable benefit of CNTs usage. The preservation of compatibility of nano-reinforced mortars, along with an enhancement in performance characteristics, is a beneficial feature for the buildings repair, ultimately prolonging their structural integrity. Furthermore, the decreased drying index, i.e. accelerated drying, of HL mortars can be utilised to address issues related to damp walls in historic buildings. Nonetheless, the potential application of nanoadditives necessitates meticulous examination on a case-by-case basis to ascertain their suitability for specific conditions. Additionally, economic factors must be evaluated to assess their applicability and cost-effectiveness.

In conclusion, the wide variety of nanomaterials, differing in dimensions, type, and chemical composition, necessitates careful selection and incorporation strategies when used as additives in construction composites. Furthermore, industrial-grade nanoadditives, which may have lower purity, may offer a similar enhancement effect and present cost advantages. Nevertheless, it is

 doi:10.20944/preprints202504.2222.v1

essential to assess their impact on material performance, as well as the specific mixing and incorporation approach, as it directly influences the final composite performance.

Future research will be designed to explore and search other alternative methods and nanoadditives to strengthen lime-based historic mortars, ensuring their suitability for heritage building restoration, while enhancing their durability and mechanical properties.

Author Contributions: Conceptualization, A.P. and Z.P.; methodology, M.P. and Z.P.; formal analysis, A.P., M.P. and Z.P.; investigation, A.P. and M.Z.; data curation, A.P., M.P. and Z.P.; writing—original draft preparation, A.P. and Z.P.; writing—review and editing, A.P., M.P. and Z.P.; supervision, M.P. and Z.P.; project administration, M.P.; funding acquisition, Z.P. All authors have read and agreed to the published version of the manuscript.

Funding: This research was funded by CZECH SCIENCE FOUNDATION, grant number 25-15998S.

Data Availability Statement: The data presented in this study are available on request from the corresponding author due to privacy.

Conflicts of Interest: The authors declare no conflicts of interest.

Abbreviations

The following abbreviations are used in this manuscript:

CL	Calcium Lime
CNT	Carbon Nanotube
GN	Graphene Nanoplatelets
HL	Hydraulic Lime
MWCNT	Multiwalled Carbon Nanotubes
NHL	Natural Hydraulic Lime
NM	Nanomaterial
PC	Portland Cement

References

1. Groot, C.; Veiga, R.; Papayianna, I.; Hees, R.H.; Secco, M.; Alvarez, J.I.; Faria, P.; Stefanidou, M. RILEM TC 277-LHS report: Lime-based mortars for restoration–a review on long-term durability aspects and experience from practice. *Mater. Struct.* **2022**, *55*, 245.
2. Elsen, J. Microscopy of historic mortars—a review. *Cem. Concr. Res.* 2006, *36(8)*, pp. 1416-1424.
3. Nogueira, R.; Pinto, A.P.F.; Gomes, A. Design and behavior of traditional lime-based plasters and renders. Review and critical appraisal of strengths and weaknesses. *Cem. Concr. Compos.* **2018**, *89*, pp. 192–204.
4. CEMBUREAU. *Activity Report 2023*; CEMBUREAU—The European Cement Association: Brussels, Belgium, 2024; pp. 29–30.
5. Loke, M.P.; Pallav, K.; Cultrone, G.; Di Filippo, C. Investigating the standard design and production procedure of heritage mortars for compatible and durable masonry restoration. *J. Build. Eng.*, **2024**, *94*, 110012.
6. Mosquera, M.J.; Silva, B.; Prieto, B.; Ruiz-Herrera, E. Addition of cement to lime-based mortars: Effect on pore structure and vapor transport. *Cem. Concr. Res.* 2006, *36(9)*, pp. 1416-1424.
7. Rakhsh Mahpour, A.; Ventura, H.; Ardanuy, M.; Rosell, J.R.; Claramunt, J. The effect of fibres and carbonation conditions on the mechanical properties and microstructure of lime/flax composites. *Constr. Build. Mater.* **2023**, *138*, 104981.
8. Klisińska-Kopacz, A.; Tišlova, R.; Adamski, G.; Kozłowski, R. Pore structure of historic and repair Roman cement mortars to establish their compatibility. *J. Cult. Herit.* **2010**, *11(4)*, pp. 404-410.
9. Ayta, A.; Bouzerd, H.; Ali-Boucetta, T.; Navarro, A.; Benmalek, M.L. Valorisation of waste glass powder and brick dust in air-lime mortars for restoration of historical buildings: Case study theatre of Skikda (Northern Algeria). *Constr. Build. Mater.* **2022**, *315*, 125681.

 doi:10.20944/preprints202504.2222.v1

10. Pacheco-Torgal, F.; Faria, J.; Jalali, S. Some considerations about the use of lime–cement mortars for building conservation purposes in Portugal: A reprehensible option or a lesser evil? *Constr. Build. Mater.* **2012**, *30*, pp. 488-494.
11. Posani, M.; Veiga, R.; De Freitas, V.P. Thermal renders for traditional and historic masonry walls: Comparative study and recommendations for hygric compatibility. *Build. Environ.* **2023**, *228*, 109737.
12. Jeevanagoudar, Y.V.; Krishna, R.H.; Gowda, R.; Preethan, R.; Prabhakara, R. Improved mechanical properties and piezoresistive sensitivity evaluation of MWCNTs reinforced cement mortars. *Constr. Build. Mater.* **2017**, *144*, pp. 188–194.
13. Dalla, P.T.; Tragazikis, I.K.; Trakakis, G.; Galiotis, C.; Dassios, K.G.; Matikas, T.E. Multifunctional Cement Mortars Enhanced with Graphene Nanoplatelets and Carbon Nanotubes. *Sensors*, **2021**, *21*, 933.
14. Chen, Y.; Li, X.; Li, C.; Zhang, N.; Liu, R.; Lu, C. Improvement of Flexural and Compressive Strength of Cement Mortar by Graphene Nanoplatelets. *Open J. Civ. Eng.* **2021**, *15*, pp. 165–171.
15. Dimou, A.-E.; Charalampidou, C.-M.; Metaxa, Z.S.; Kourkoulis, S.K.; Karatasios, I.; Asimakopoulos, G.; Alexopoulos, N.D. Me-chanical and electrical properties of hydraulic lime pastes reinforced with carbon nanomaterials. *Procedia Struct. Integr.* **2020**, *28*, pp. 1694–1701.
16. Dimou, A.-E.; Metaxa, Z.S.; Alexopoulos, N.D.; Kourkoulis, S.K. Assessing the potential of nano-reinforced blended lime-cement pastes as self-sensing materials for restoration applications. *Mater. Today*, **2022**, *62*, pp. 2482–2487.
17. Faria, P.; Duarte, P.; Barbosa, D.; Ferrira, I. New composite of natural hydraulic lime mortar with graphene oxide. *Constr. Build. Mater.* **2017**, *156*, pp. 1150–1157.
18. Nguyen, V. S.; Rouxel, D.; Vincent, B. Dispersion of nano-particles: From organic solvents to polymer solutions. *Ultrason. Sonochem.* **2014**, *21(1)*, pp. 149–153.
19. Debbarma, K.; Debnath, B. and Sarkar, P.P. A comprehensive review on the usage of nanomaterials in asphalt mixes. *Constr. Build. Mater.* **2022**, *361*, 129634.
20. Zhou, N.; Wang, S.; Walsh, F.C. Effective particle dispersion via high-shear mixing of the electrolyte for electroplating a nickel-molybdenum disulphide composite. *Electrochim. Acta.* **2018**, *283*, pp. 568–577.
21. Kaur, I.; Ellis, L.-J.; Romer, I.; Tantra, R.; Carriere, M.; Allard, S.; Mayne-L'Hermite, M.; Minelli, C.; Unger, W.; Potthoff, A.; Rades, S; Valsami-Jones, E. Dispersion of Nanomaterials in Aqueous Media: Towards Protocol Optimization. *J. Vis. Exp.* **2017**, *130*, 56074.
22. Tantra, R.; Oksel, C.; Robinson, K.N.; Sikora, A. ; Wang, X.Z.; Wilkins, T.A. A method for assessing nanomaterial dispersion quality based on principal component analysis of particle size distribution data. *Particuology*, **2015**, *22*, pp. 30–38.
23. Lau, K.; Lu, M.; Lam, C.; Cheung, H.; Sheng, F.; Li, H. Thermal and mechanical properties of single-walled carbon nanotube bundle-reinforced epoxy nanocomposites: the role of solvent for nanotube dispersion. *Compos. Sci. Technol.* **2005**, *65(5)*, pp. 719-725.
24. Asadi, A.; Pourfattah, F.; Miklós Szilágyi, I.; Afrand, M.; Żyła, G.; Ahn, H.S.; Wongwises, S.; Nguyen, H.M.; Arabkoohsar, A.; Mahian, O. Effect of sonication characteristics on stability, thermo-physical properties, and heat transfer of nanofluids: A comprehensive review. *Ultrason. Sonochem.* **2019**, *58*, 104701.
25. Moshiul Alam, A.K.M. Methods of nanoparticle dispersion in the polymer matrix. In *Nanoparticle-Based Polymer Composites*, Rangappa, S.M., Parameswaranpillai, J., Gowda, T.G.Y., Siengchin, S, Seydibeyoglu, M.O. Publisher: Woodhead Publishing, Sawston, United Kingdom, 2022, pp. 469-479.
26. Azunna, S.U.; Aziz, F.N.A.B.A.; Al-Ghazali, N.A.; Rashid, R.S.M.; Bakar, N.A. Review on the mechanical properties of rubberized geopolymer concrete. *Clean. Mater.* **2024**, *11*, 100225.
27. Lauermannová, A.-M.; Jankovský, O.; Jiříčková, A.; Sedmidubský, D.; Záleská, M.; Pivák, A.; Pavlíková, M.; Pavlík, Z. MOC Composites for Construction: Improvement in Water Resistance by Addition of Nanodopants and Polyphenol. *Polymers* **2023**, *15*(21), 4300.
28. *EN 459-2*; Building lime—Part 2: Test Methods. CEN: Brussels, Belgium, 2021.
29. Selvam, C.; Mohan Lal, D.; Harish, S. Enhanced heat transfer performance of an automobile radiator with graphene based suspensions. *Appl. Therm. Eng*. **2017**, *123*, pp. 50–60.

 doi:10.20944/preprints202504.2222.v1

30. Zaman, A.C.; Kaya, F.; Kaya, C. A study on optimum surfactant to multiwalled carbon nanotube ratio in alcoholic stable suspensions via UV–Vis absorption spectroscopy and zeta potential analysis. *Ceram. Int.* **2020**, *46*, pp. 29120–29129.
31. Lauermannová, A.-M..; Lojka, M.; Sklenka, J.; Záleská, M.; Pavlíková, M.; Pivák, A.; Pavlík, Z.; Jankovský, O. Magnesium oxychloride-graphene composites: Towards high strength and water resistant materials for construction industry. *FlatChem*, **2021**, *29*, 100284.
32. Petkova, B.; Tcholakova, S.; Denkov, N. Foamability of surfactant solutions: Interplay between adsorption and hydrodynamic conditions. *Colloids Surf. A: Physicochem. Eng. Asp.*, **2021**, *626*, 127009.
33. Kapicová, A.; Pivák, A.; Záleská, M.; Pavlíková, M.; Pavlík, Z. Influence of different surfactants on hydrated lime pastes modified with CNTs. In Proceedings of the International Conference of Numerical Analysis and Applied Mathematics Icnaam 2021, Rhodes, Greece, 20–26 September 2021.
34. *EN 1015-1*; Methods of Test for Mortar for Masonry—Part 1: Determination of Particle Size Distribution (by Sieve Analysis). CEN: Brussels, Belgium, 1999.
35. *EN 1015-3*; Methods of Test for Mortar for Masonry—Part 3: Determination of Consistence of Fresh Mortar (by Flow Table). CEN: Brussels, Belgium, 2000.
36. *EN 1015-10*; Methods of Test for Mortar for Masonry—Part 10: Determination of Dry Bulk Density of Hardened Mortar. CEN: Brussels, Belgium, 2000.
37. *EN 1015-11*; Methods of Test for Mortar for Masonry—Part 11: Determination of Flexural and Compressive Strength of Hardened Mortar. CEN: Brussels, Belgium, 2020.
38. *EN 12504-4*; Testing Concrete in Structures—Part 4: Determination of Ultrasonic Pulse Velocity. CEN: Brussels, Belgium, 2021.
39. *EN 1015-18*; Methods of Test for Mortar for Masonry—Part 18: Determination of Water Absorption Coefficient Due to Capillarity Action of Hardened Mortar. CEN: Brussels, Belgium, 2003.
40. Pavlík, Z.; Černý, R. Determination of moisture diffusivity as a function of both moisture and temperature. *Int. J. Thermophys.* **2012**, *33*, pp. 1704–1714.
41. *EN 16322*; Conservation of Cultural Heritage—Test Methods—Determination of Drying Properties. CEN: Brussels, Belgium, 2013.
42. Han, Z.; Fina, A. Thermal conductivity of carbon nanotubes and their polymer nanocomposites: A review. *Prog. Polym. Sci.* **2011**, *36*, pp. 914-944.
43. Vyšvařil, M.; Pavlíková, M.; Záleská, M.; Pivák, A.; Žižlavský, T.; Rovnaníková, P.; Bayer, P.; Pavlík, Z.; on-hydrophobized perlite renders for repair and thermal insulation purposes: Influence of different binders on their properties and durability. *Constr. Build. Mater.* **2020**, *263*, 120617.
44. Gonçalves, T.D.; Brito, V. Artisanal Lime Coatings and Their Influence on Moisture Transport During Drying. In Historic Mortars; Hughes, J., Válek, J., Groot, C., Eds.; Springer: Cham, Switzerland, **2019**; pp. 241–253.
45. Salomão, M.C.dF.; Bauer, E.; Kazmierczak, C.d.S. Drying parameters of rendering mortars. Ambiente Construido **2018**, *18*, pp. 7–19.
46. Flores-Colen, I.; Silva, L.; de Brito, J.; de Feritas, V.P. Drying index for in-service physical performance assessment of renders. *Constr. Build. Mater.* **2016**, *112*, pp. 1101–1109.
47. Scheffler, G.A.; Plagge, R.; Introduction of a Drying Coefficient for Building Materials. ASHRAE Transactions **2010**, *116*.